

Next-generation RNA sequencing reveals differential expression of MYCN target genes and suggests the mTOR pathway as a promising therapy target in *MYCN*-amplified neuroblastoma

Alexander Schramm<sup>1</sup>, Johannes Köster<sup>1,2</sup>, Tobias Marschall<sup>3,4</sup>, Marcel Martin<sup>4</sup>, Melanie Heilmann<sup>1</sup>, Kathrin Fielitz<sup>1</sup>, Gabriele Büchel<sup>1</sup>, Matthias Barann<sup>5</sup>, Daniela Esser<sup>5</sup>, Philip Rosenstiel<sup>5</sup>, Sven Rahmann<sup>2,4</sup>, Angelika Eggert<sup>1</sup> and Johannes H. Schulte<sup>1</sup>

**Authors affiliation:**

1 Department of Pediatric Hematology and Oncology, University Children's Hospital, Essen, Germany;

2 Department of Genome Informatics, University Hospital Essen, Essen, Germany

3 CWI Amsterdam, Statistical Modeling and Comparative Genomics Group  
Amsterdam, The Netherlands

4 Department of Computer Science, LS11, University of Dortmund

5 Institute of Clinical Molecular Biology, Christian Albrechts University Kiel, Germany

**Contact information:**

PD Dr. Alexander Schramm

University Childrens Hospital Essen

Department of Pediatric Hematology and Oncology

Hufelandstr. 55, 45122 Essen

Email: alexander.schramm@uni-due.de

Tel : +49 201 7232506

Fax : +49 201 7235750

**Novelty & Impact Statements**

Next-generation RNA sequencing is a valuable tool for linking changes inherent to a cancer genome to its transcribed counterpart. Cancer-specific transcriptome changes will facilitate the selection of individualised treatment strategies. Here, we describe the coding transcriptome of 20 primary neuroblastomas, a tumor of early childhood, by RNA deep sequencing. We identify genes and pathways associated with *MYCN* in vivo and in vitro and suggest the mTOR pathway as a therapeutic target for *MYCN*-amplified neuroblastoma.

## Abstract

In many cancer types, MYC proteins are known to be master regulators of the RNA-producing machinery. Neuroblastoma is a tumor of early childhood characterised by heterogeneous clinical courses. Amplification of the *MYCN* oncogene is a marker of poor patient outcome in this disease. Here, we investigated the *MYCN*-driven transcriptome of 20 primary neuroblastomas with and without *MYCN* amplification using next-generation RNA sequencing, and compared the results to those from an in vitro cell model for inducible *MYCN* (SH-EP *MYCN*-ER). Transcriptome sequencing produced 30 - 90 million mappable reads for each dataset. The most abundant RNA species was mRNA, but snoRNAs, pseudogenes and processed transcripts were also recovered. A total of 223 genes were significantly differentially expressed between *MYCN*-amplified and single-copy tumors. Of those genes associated with *MYCN* both in vitro and in vivo, 32% of *MYCN* upregulated and 37% of *MYCN* downregulated genes were verified either as previously identified *MYCN* targets or as having *MYCN*-binding motifs. Pathway analyses suggested transcriptomal upregulation of mTOR related genes by *MYCN*. *MYCN*-driven neuroblastomas in mice displayed activation of the mTOR pathway on the protein level and activation of *MYCN* in SH-EP *MYCN*-ER cells resulted in high sensitivity towards mTOR inhibition in vitro. We conclude that next-generation RNA sequencing allows for the identification of *MYCN* regulated transcripts in neuroblastoma. As our results suggest *MYCN* involvement in mTOR pathway activation on the transcriptional level, mTOR inhibitors should be further evaluated for the treatment of *MYCN*-amplified neuroblastoma.

## Introduction

Neuroblastoma (NB) is a cancer of childhood presenting with extreme courses: while aggressive NB still poses a challenge to clinicians and recurrent disease renders an infaust prognosis despite multimodal therapy <sup>1</sup>, intermediate-risk patients with favourable tumor biology can be successfully treated with a less intensive treatment <sup>2</sup>. Moreover, benign neuroblastic tumors can be cured by surgery combined with a “wait-and-see” strategy <sup>3</sup>. Many efforts have been undertaken to identify risk factors for aggressive neuroblastoma, but amplification of the *MYCN* oncogene is still the most powerful single predictor of adverse outcome of NB <sup>4</sup>. *MYCN* amplification is observed in about 20% of all NB patients and is usually associated with fatal outcome of the disease <sup>5</sup>. As *MYCN* is a transcription factor, thus not representing an ideal druggable target, molecular analyses of this subgroup of NB promises to result not only in a better understanding of *MYCN* driven tumor biology but also in novel treatment options for this most aggressive tumor subtype.

With the onset of affordable next-generation sequencing (NGS) technologies, it can be anticipated that underlying gene mutations for every tumor will be identified within the next few years. For NB, first reports on the mutational spectrum of the disease have been recently published <sup>6</sup>, stressing the importance of *MYCN*, chromosomal stability and mutations in neuritogenesis genes for neuroblastoma development. In neuroblastoma, a genetic association with the onset of the disease has only been found for a small fraction of all cases. Activating mutations in the coding gene for anaplastic lymphoma kinase (*ALK*) have been described in about eight percent of all NB patients <sup>7-11</sup>, while mutations in the *PHOX2B* gene, which is also associated with Hirschsprung disease, are even less frequent (1-2% <sup>12, 13</sup>). Therefore, the vast majority of neuroblastomas are sporadic cases with a heterogeneous mutational spectrum. In the light of endeavours to treat patients according to their individual risk profile, these heterogeneity could imply that risk factors such as *MYCN* amplification or loss of chromosome 11q <sup>14, 15</sup> will still have an impact on the choice of individualised treatment. Moreover, the impact of the “mutanome” as the sum of all cancer-associated genetic changes on transcriptomal alterations remains to be explored.

We have previously reported on tumor-associated changes in the small RNA transcriptome of primary neuroblastoma thus describing the entire spectrum of NB-

associated miRNAs<sup>16</sup>. The oncogenic or tumor-suppressive functions of these miRNAs could be verified by independent methods and experiments<sup>17, 18</sup> exemplifying that the results from next-generation sequencing can be meaningfully exploited for functional studies.

Here, we focused on the coding transcriptome of primary NB by comparing absolute RNA expression levels in tumor samples from patients with and without *MYCN* amplification using next-generation RNA sequencing. In order to identify direct *MYCN* targets we also included an NB cell line with inducible induction of *MYCN* in the sequencing pipeline. The intersection of regulated genes between the in vivo and the in vitro samples was anticipated to include genes, whose expression is tightly linked or directly regulated by *MYCN*. With this information at hand it was expected that *MYCN* gene regulatory networks as well as potential targets for *MYCN*-driven NB could be identified.

## Material and Methods

### Cell culture and in vitro analyses

Cultivation of human neuroblastoma cells SH-EP, SH-EP MYCN-ER and WAC2 was performed as previously described<sup>19</sup>. SH-EP is a MYCN null neuroblastoma cell line and genetically identical to SH-SY5Y but displaying an epithelium-like phenotype<sup>20</sup>. WAC2 is a subclone of SH-EP engineered to stably overexpress MYCN<sup>21</sup>. Activation of MYCN in SH-EP MYCN-ER was achieved using 4-hydroxy tamoxifen and confirmed after 72 h by detecting transcriptional induction of the MYCN-target gene, ODC-1, as described<sup>19</sup>. Cell viability following treatment with BEZ-235 (Axon Medchem, Groningen, The Netherlands) was measured using MTT (3-(4,5-dimethylthiazol-2-yl)-2,5-diphenyltetrazoliumbromide) as previously described<sup>22</sup>.

### RNA preparation for next generation sequencing

NB patients included in this study were from German trials NB 97 or 2004, respectively. Representative areas of histologically confirmed, snap-frozen NB were cut on dry ice. No preselection for tumor cell fraction or microenvironment was performed. Total RNA extraction of NB tumor samples and cell lines described above was performed by silica gel-based membrane purification methods (RNeasy Mini kit or MicroRNeasy kit, Qiagen, Hilden, Germany) according to the manufacturer's instructions. Depletion of ribosomal RNAs was achieved using the RiboMinus Human Transcriptome Kit (Invitrogen, Carlsbad, CA) according to the manufacturer's instructions. RNA quality as well as rRNA depletion efficiency was controlled by capillary gel electrophoresis using the Bioanalyser 2100 (RNA nano kits, Agilent).

### Library generation and transcriptome sequencing

Library preparation was performed as previously described<sup>23</sup>. Of the depleted rRNA, 50-500 ng was used as input for the whole transcriptome analysis kit (Applied Biosystems, Carlsbad, CA). Library preparation was performed according to the manufacturer's protocol. Sequencing was performed using the SOLiD "Top Paired End Seq DNA Frag Kit MM 50/35 v4" (Applied Biosystems, Carlsbad, CA) on the SOLiD V4 platform. In total 24 libraries were generated and sequenced.

### Sequence processing and mapping

SOLiD reads were mapped to the Human Genome RefSeq Hg19 using Bioscope v1.21. A clearzone of 5.0 and mismatch penalty of -2.0 were set, and a repetitive mapping was performed using the following settings: 38.3.0, 25.2.0 (anchorLength.mismatchAllowed.anchorStart). See the “Bioscope Userguide” for a more detailed description of the Bioscope mapping algorithm. For ambiguous mappings, only the alignment with best mapping quality was considered. Based on the ENSEMBL Hg19 annotation (rev. 63), per gene expression values were set as the maximum coverage of the exonic gene regions.

### **Normalization**

Gene expressions were normalized to allow comparison across datasets. A qq-scale normalization as described in <sup>16</sup> was performed separately for the tumor samples and the in vitro datasets. Quantile-quantile (qq) plots of the distribution of gene expression values of each dataset against one arbitrarily chosen reference dataset were compared. By considering only the 75-95% quantiles, robustness against less abundant genes and outliers was ensured. With the scaling factor given by the median of differences between these quantiles, a purely linear transformation was performed <sup>16</sup>.

### **Statistical testing and cluster analysis**

Statistical analysis and clustering of gene expressions was performed using R 2.14 (<http://www.r-project.org>). Genes were tested for differential expression using MYCN status (amplified vs normal) or survival (see supplemental table 1 for patient characteristics) as variables. For each gene, the fold change was computed as the ratio of the mean gene expressions of the classes, while fold changes between 1 and 0 were replaced by the negative of their inverse. In the tumor datasets, genes with a p-value < 0.05 and an absolute fold change of at least 1.5 were considered to be significantly differentially expressed. The false discovery rate (FDR) was calculated using Benjamini–Hochberg multiple testing correction using the R library “multtest” <sup>24</sup>; <sup>25</sup>. Hierarchical clustering was performed based on Canberra distances <sup>16</sup>.

### **In silico verification of potential MYCN targets**

A list of potential MYCN targets was obtained by selecting genes that were significantly differentially expressed using MNA classification in the tumor, and

exhibited an absolute fold change of at least 1.5 in the in vitro datasets. Potential targets were verified using existing databases (MYC target gene database, <http://www.mycancergene.org>,<sup>26</sup> and the MYCNot Database [<http://medgen.ugent.be/MYCNot>]). Further, the MYCN binding motif E-Box (CACGTG), together with its isoforms (CATGTG, CATTTG, CATCTG, CAACTG) reported by<sup>27</sup> was tested for significant overrepresentation ( $p \leq 0.05$ ) in the promoter regions of the genes. Therefore, each motif was tested in a 1000 base region upstream of the first exon of each gene using the sequence alignment tool MosDi (<http://code.google.com/p/mosdi/>,<sup>28</sup>).

### **Confirmation of mTOR pathway activation in tumors from TH-MYCN mice**

TH-MYCN mice were housed in the central animal facility of the University Hospital Essen. These mice developed neuroblastoma at a frequency comparable to published data<sup>29</sup>. Total protein was isolated from tumors and normal livers of three tumor-bearing animals. Western Blot analysis was performed to detect total Akt, phospho-Akt, total p70S6K and phospho-p70S6K to evaluate Akt/mTOR pathway activation. All primary antibodies were obtained from Cell Signaling (Beverly, MA).

## Results

Following RNA isolation and rRNA depletion, transcriptomes from 20 primary NB with and without *MYCN* amplification and a NB cell line with and without induction of *MYCN* (SH-EP *MYCN*-ER) were analyzed by NGS using paired-end sequencing on a SOLiD4 sequencer (Applied Biosystems). Patient characteristics are listed in supplemental table 1. Mapping against the human genome RefSeq Hg19 was performed using BioScope (see methods). On average, 31.615.883 reads for each tumor, and 89.689.520 reads for each in vitro dataset could be mapped to the reference genome. The most abundant class of RNA species were protein coding mRNAs, followed by snoRNAs, pseudogenes and processed transcripts, which are non-coding transcripts without an open reading frame (fig. 1). The distribution of RNA species underscores both the efficiency for rRNA depletion and mRNA enrichment in our samples.

All transcripts were mapped to the ENSEMBL Hg19 annotation containing 53717 features including coding genes. Of those, 8030 coding genes were found to have absolute expression counts >10 in at least five samples. To obtain comparable expression values, a qq-scale normalization among all tumor datasets was performed (see methods, fig. 2A, B) and expression values were then calculated for all tumor datasets (see methods). We first focused on differential expression analysis in order to find gene expression patterns as well as individual genes with significant expression differences between *MYCN*-amplified and *MYCN* single copy tumors or expression patterns associated with survival. Only genes with an absolute expression count of at least 10 in at least five tumor datasets were selected for these analyses. Based on our filter criteria, 945 and 727 genes were used for classification according to *MYCN* status or survival, respectively, and p-values for differential expression were calculated. A total of 223 genes were significantly differentially expressed between patients with *MYCN* amplification and patients with normal *MYCN* status. For patients surviving their disease for more than three years without an event, 211 genes were found to be significantly different when compared to the patients succumbing to their disease. To address the problem of multiple testing, we plotted the distribution of p-values to evaluate if low p-values were over-represented between the different groups. Indeed, there is an enrichment of low p-values when gene expression was compared for patients with or without *MYCN* amplification and

those surviving the disease to those who succumbed (fig. 2C, D). This finding implies that there are true transcriptomal differences between these groups.

Looking at the most differentially expressed transcripts considering *MYCN* amplification (fig. 3A) or survival (fig. 3B) both upregulation and downregulation of candidate *MYCN* targets could be detected. Mostly, we observed regulation of protein coding mRNAs, but also differential expression of snoRNAs including *SNORA71C* and *SNORD116* was observed. An unsupervised hierarchical clustering using all significantly differentially expressed genes resulted in a perfect separation between *MYCN* amplified and *MYCN* normal patients (fig. 3C). When trying to separate patients according to survival based on the list of significantly differentially expressed transcripts, we noticed that there was one misclassification (fig. 3D). Taken together, the principled differences between the transcriptomes of aggressive and less aggressive neuroblastomas allowed for the separation of these clinically divergent groups.

Genes and transcripts with significant differential expression dependent on the *MYCN* amplification status are candidate direct or indirect *MYCN* targets. To obtain insights into a direct *MYC* regulation of the transcripts that were identified in the primary tumors, a well-established model system of inducible *MYCN* function in a neuroblastoma cell line, SH-EP *MYCN*-ER, was used. In this model system, *MYCN* is expressed in a cell line without endogenous *MYCN* as a fusion gene with the estrogen-responsive domain of the ER receptor. *MYCN* activation can only be induced in the presence of 4-hydroxy-tamoxifen causing a nuclear translocation of the *MYCN*-ER fusion protein. The transcriptome of SH-EP *MYCN*-ER cells with or without induction of functional *MYCN* was analysed by RNA sequencing as described for the primary tumors and differentially expressed transcripts in the presence or absence of functional *MYCN* were identified accordingly. The list of transcripts associated with *MYCN* amplification in vivo and transcripts induced by *MYCN* in vitro were then compared to narrow down the candidate genes directly targeted by *MYCN*. For this purpose, we first omitted all genes that had a fold change (either up or down) of less than 1.5 in vitro. Second, we kept only those genes, for which the sign of the fold change (i.e. the direction of regulation) was the same in tumors and in vitro. Application of these filter criteria resulted in 25 genes that were upregulated (positive fold change) and 19 genes that were downregulated (negative fold change) upon *MYCN* induction in vitro (figs. 4A and S2) and *MYCN* amplification (figs. 4B and S2).

Among the upregulated genes, we found 3 known MYCN targets as described in publicly available databases (see methods). Interestingly, we also identified 7 MYCN target genes to be downregulated. Homology searches identified an E-Box binding motif, which is the MYCN transcription factor binding site, in the promoter region of 5 upregulated genes and 1 downregulated gene (table 1, see methods), implying that these genes are also bona-fide direct MYCN targets. In total, 32% of the upregulated and 37% of the downregulated genes could be verified as either known MYCN targets or novel targets containing E-boxes.

We first validated upregulation of the top-ranked target genes hexokinase 2 (HK2) and BZW2 in the SH-EP MYCN-ER model system as well as in a SH-EP subclone, designated WAC2, which is engineered to stably overexpress MYCN<sup>21</sup>. Upregulation of HK2 as well as BZW2 mRNA by real-time PCR could be seen in both of the in vitro systems with forced expression of MYCN. HK2 and BZW2 expression were also found to correlate with MYCN amplification in an independent cohort of 113 neuroblastoma patients profiled by Affymetrix HuEXST1.0 arrays (Schramm et al., submitted, figs. 4C, E). Taken together, reanalyses of microarray data from primary NB confirmed that HK2, BZW2 and RPTOR are significantly correlated with MYCN amplification. These data exemplify that the MYCN targets identified here by sequencing can also be validated by independent methods.

We next focused on classification of MYCN targets genes to better understand the molecular processes regulated by MYCN in neuroblastoma. For these purpose, we looked into GO and KEGG databases to identify pathways significantly associated with MYCN. Analyses of over-representation of genes within a pathway indicated that MYCN significantly modulated genes involved in protein biosynthesis and the mTOR pathway. GO analyses revealed that genes coding for ribosomal subunits, as well as genes involved in “ribonucleoprotein complexes” were significantly enriched and upregulated both in vitro and in vivo by MYCN (fig. 5A, p-value <0.001). KEGG pathway analyses confirmed these association and implied that three genes of the mTOR pathway, REDD1/DDIT4, 4EBP1 and RPTOR, were significantly altered by the MYCN status in vivo and in vitro (fig. 5B and supplemental table 2, adjusted p-value:  $8 \times 10^{-4}$ ). A significant correlation between RPTOR expression and MYCN amplification could also be seen in an independent panel of primary neuroblastoma (supplemental figure 2). We therefore decided to look for mTOR pathway activation in a model of MYCN-driven neuroblastoma, the TH-MYCN mouse<sup>29</sup>. In this model

system, we used phosphorylation of the S70 kinase and AKT as a readout of AKT/mTOR activation in the MYCN-driven tumors. Indeed, we could demonstrate tumor-specific activation of the mTOR pathway in tumors obtained from TH-MYCN mice compared to normal tissue from the same mice (fig. 5C). To test, whether up-regulation of mTOR pathway genes was concomitant with sensitivity to mTOR inhibition, we performed in vitro proliferation assays using the mTOR inhibitor BEZ-235, which is currently in late phase of clinical development. Sensitivity to BEZ-235 was comparable between SH-EP and WAC2 cells and even more pronounced in SH-EP MYCN-ER cells upon MYCN activation (fig. 5D, SH-EP MYCN+). Thus, we could link two cancer-relevant pathways, protein biosynthesis and the mTOR pathway to the MYCN status in neuroblastoma by using transcriptome NGS.

## Discussion

Deciphering cancer genomes and transcriptomes is estimated to yield a wealth of information, which can be exploited for modelling tumorigenesis as well as for setting up individualised treatment of cancer patients. Reports available so far have established a correlation between mutational frequency in cancer, patient age and exposition to potentially carcinogenic agents such as UV-light or smoking. This complicates the hunt for the driving mutational events given a high background of acquired passenger mutations. Moreover, intratumoral heterogeneity could further complicate the design of rationale, individualised treatment options<sup>30</sup>. In those childhood tumors, for which entire genomes have been sequenced, such as medulloblastoma<sup>31</sup>, retinoblastoma<sup>32</sup> and neuroblastoma<sup>6</sup>, patients have significantly lower numbers of mutations compared to adult tumors. This should in principle facilitate the search for the tumor driving events, at least for the sporadic forms of the disease. Still, the route from the tumor genome to the tumor phenotype demands analyses of the intermediate steps including alterations in the tumor transcriptome. RNA profiles can be expected not only to include signatures but also to give valuable hints on aberrantly activated signalling pathways in tumors, which can be used for targeted therapies. As a first step towards this direction, we here describe for the first time the entire transcriptome of 20 primary NB using next-generation sequencing. Since we previously described the non-coding transcriptome of NB<sup>16</sup>, we here focused on protein-coding transcripts and identified genes and patterns associated with the most aggressive NB subtype, characterised by amplification of the *MYCN* oncogene. As expected, mRNA was identified as the predominant RNA species following annotation of sequences obtained by RNA-NGS, but we could also detect a considerable amount of snoRNAs, whose function is presently poorly understood. Previous reports have also linked expression of ncRNAs/snoRNAs as well as miRNAs to *MYCN* amplification<sup>19, 33</sup> and it was shown that *MYCN* expression itself is controlled by miRNAs<sup>34</sup>. It is speculated that ncRNAs can function in regulating gene expression, which is also of functional importance in developmental processes as well as in cancer progression<sup>35-37</sup>. Thus, the non-coding part of the transcribed regions of the genome can be expected to harbour an additional layer of regulation to gene expression in addition to miRNAs in neuroblastoma and other tumors.

Analyses of the most divergently expressed transcripts between *MYCN*-amplified and *MYCN*-single copy tumors confirmed the principled differences between these two groups, which has also been pointed out before<sup>38, 39</sup>. Hierarchical clustering using these differentially expressed transcripts as input revealed a perfect separation of patients with and without *MYCN* amplification, emphasizing the homogeneity of discriminative patterns (fig. 3C).

Although the sequencing depth achieved in our approach was not sufficient to cope with alternative transcript use, we were able to identify differentially expressed transcripts associated with *MYCN* in vivo and regulated by *MYCN* in vitro in a NB model system with inducible *MYCN* (fig. 4). The most prominently regulated target, *HK2*, was validated both in an independent cohort of primary neuroblastomas as well as in an NB in vitro model with inducible nuclear *MYCN* translocation, SH-EP *MYCN*-ER. Induction of *HK2* as well as other targets of the glycolytic pathway has been recently associated with the *MYCN*-mediated Warburg effect in neuroblastoma<sup>40</sup>. Functional significance of other targets, especially the snoRNAs, which are upregulated both in vitro and in vivo by *MYCN* remains to be determined.

Analyses of associated pathways using GO and KEGG databases linked protein biosynthesis and the mTOR pathway to *MYCN*-upregulated genes in NB and these were also positively correlated with *MYCN* amplification in primary tumors. Protein biosynthesis has also been reported to be induced by *MYCN* in vitro before in an unbiased approach using SAGE technology<sup>41</sup> and this was verified in this study also for primary tumors. In a previous array based study, cell cycle genes and genes involved in kinetochore assembly had been associated with survival and *MYCN* amplification in primary NB, but these genes have not been verified using NB in vitro models<sup>42</sup>. By contrast, we found three genes from the mTOR pathway to be upregulated by *MYCN*, which strongly supports the notion that the mTOR/PI3K/Akt axis is an important feature of *MYCN*-driven survival capabilities of tumor cells. It could also be shown that interference with this pathway in turn leads to the degradation of *MYCN* protein in neuroblastoma using small molecule inhibitors of mTOR such as rapamycin or novel drugs such as BEZ-235 currently in clinical development<sup>43, 44</sup>. We here demonstrated tumor-specific activation of the mTOR pathway in a *MYCN*-driven neuroblastoma mouse model. Furthermore, we confirmed that neuroblastoma cells are sensitive towards mTOR-directed treatment, in line with a previous report demonstrating *MYCN* downregulation in neuroblastoma cells upon

mTOR inhibition<sup>43</sup>. Here, we show that especially in cells with overexpression or activation of MYCN mTOR inhibition might be appropriate to effectively block proliferation.

Taken together, we here provide first insights into the transcriptomal landscape of *MYCN*-amplified neuroblastoma using next-generation RNA sequencing. We have identified genes and pathways including coding mRNAs as well as non-coding RNAs associated with MYCN in vivo and in vitro. Our results strongly argue in favour of further evaluation of mTOR inhibitors for the treatment of *MYCN*-amplified NB.

## Legends to tables and figures

### Table 1

Intersection of MYCN targets identified both in vitro in a NB cell culture model upon MYCN induction and from the in vivo comparison of differentially expressed transcripts between MYCN-amplified and MYCN single copy patients. The genes listed here were either previously described in public databases designated MycDB<sup>26</sup> and MYCNot or identified by MoSDi, a motif software described elsewhere<sup>28</sup>, which was here used to recognise overrepresentation of MYCN-binding motifs in the promoter region of target genes (E-box like sequences are put in parentheses).

### Fig. 1

Distribution of RNA species for the samples sequenced by NGS. Note that the predominant form is mRNA (light blue), but that also lincRNAs, snoRNAs and snRNAs were readily detectable, although at lower levels. Immunoglobulin pseudogenes and miRNAs (subsumed in white) are only present in minor amounts due to the size selection and depletion strategy. “MYCNsc” and “MNA” refers to samples from *MYCN* single-copy or *MYCN*-amplified patients, respectively. “SH-EP MYCN-ER” refers to samples from the SH-EP MYCN-ER cell line before (“-”) and after induction of MYCN (“+”) by 4-OHT. Transcriptomes of cell lines were analysed in duplicate from independent biological samples.

### Fig. 2

Effects of normalization on transcriptome comparability. A qq-normalization was performed separately for in vivo (A) and in vitro (B) samples, using the quantiles between 75% and 95% to ensure robustness. Histogram of uncorrected p-values after testing equality of expression count means for each RNA between *MYCN*-amplified vs *MYCN* single copy tumors (C) or patients who died from their disease vs patients who survived (D). Distribution of P-values is expected to be uniformly distributed across the unit interval (blue line), when data with equal means were compared. Here, P-values <0.05 (red line) are enriched, indicating significant differences between the groups analysed.

**Fig. 3**

Significantly different expressed genes in tumor samples grouped by MYCN status (A) or survival (B). The 40 genes with the lowest uncorrected p-values are presented as strip chart of normalised read count. Blue crosses represent expression values in MYCN single copy (A) and surviving patients (B), respectively. Red crosses depict expression values in *MYCN*-amplified (A) and deceased patients (B), respectively. Heat map and cluster dendrogram of all significant ( $p < 0.05$ ) RNAs differentially expressed between *MYCN*-amplified vs. *MYCN* single copy patients and surviving patients vs. deceased, respectively. Note that the *MYCN* status allows for perfect separation, while the classification according to survival yields one wrongly assigned sample. Clustering was based on Canberra distance and single-linkage clustering.

**Fig. 4**

Significantly differentially expressed genes between *MYCN*-amplified tumors and *MYCN* normal tumors verified in an in vitro NB model with inducible MYCN expression. Data are presented as strip charts of normalised read count as pairwise comparison of genes that are upregulated upon MYCN induction in vitro (A) and positively correlated with *MYCN* amplification in vivo (B). Blue colour depicts data from the NB in vitro system without MYCN induction (A) or from *MYCN* normal tumors (B). Red colour depicts data from the NB in vitro system with MYCN induction (A) or from tumors with *MYCN* amplification (B). The top target genes HK2 and BZW2 are upregulated in *MYCN*-amplified tumors in an independent cohort of primary NB analyses using exon-level expression analyses (C, E, Schramm et al., submitted). Numbers refer to the probe sets for the respective genes on the array. HK2 and BZW2 mRNA are also upregulated in two in vitro NB models, upon overexpression or induction of MYCN, respectively (D, F). Displayed are the fold changes of normalised HK2 and BZW2 mRNA expression measured by semi-quantitative RT-PCR in MYCN-overexpressing WAC2 cells compared to the parental cell line SH-EP and in SH-EP MYCN-ER cells following MYCN activation (SH-EP MYCN+) compared to cells without induction of MYCN (SH-EP MYCN-).

**Fig. 5**

(A) Gene ontology (GO) analyses revealed a significant association of genes upregulated in tumors from patients with MYCN amplification with GO terms for

protein biosynthesis (marked in dark grey). (B) KEGG pathway analyses returns a significant association of genes upregulated in tumors from patients with MYCN amplification with the mTOR pathway (genes marked in dark grey are upregulated in MYCN-amplified tumors). (C) Activation of Akt/mTOR pathway is seen in tumors (tu) from MYCN-driven murine neuroblastoma but not in control tissue (liver= li). (D) Sensitivity to mTOR pathway inhibition using BEZ-235 is high in neuroblastoma cells and comparable between parental SH-EP cells (open squares, IC50= 29 nM) compared to those with enforced expression (WAC2, open circles, IC50= 28 nM) with slightly increased sensitivity upon activation of MYCN (SH-EP MYCN+, open triangles, IC50= 12 nM).

### Supplemental table 1

Clinical and molecular data for neuroblastoma patients, for whom RNA expression data were obtained by NGS. The columns depict the *INSS Stage*, the *age at diagnosis* in months (mo), the status of the MYCN oncogene *MNA*= 1, MYCN amplification, *MNA*= 0, MYCN normal. *DoD* is “1” if patients died from their disease and “0”, if patients survived. Only true survivors were included, therefore none of the patient annotated as “0” died from other causes. *OS* and *EFS* depict the overall and event-free survival, respectively, presented as days since diagnosis.

### Supplemental table 2

Results of KEGG pathway analyses for genes, which are significantly upregulated in MYCN-amplified patients. For each KEGG pathway, the first row lists the KEGG pathway name, and corresponding KEGG ID. The second row lists number of reference genes in the category (C), number of genes in the gene set and also in the category (O), expected number in the category (E), Ratio of enrichment (R), p value from hypergeometric test (rawP), and p value adjusted by the multiple test adjustment (adjP). Finally, genes in the pathway are listed. For each gene, the table lists the user uploaded ID and value (optional), Entrez ID, Ensembl Gene Stable ID, Gene symbol, and description. Ensembl Gene Stable ID and Entrez Gene ID are linked to the Ensembl and Entrez Gene databases, respectively. Note that “ribosome” and “mTOR signalling pathway” are most significantly linked to MYCN amplification.

### Supplemental figure 1

Strip charts of genes that are significantly downregulated upon MYCN induction in vitro (A) and negatively correlated with *MYCN* amplification in vivo (B). Only genes with a fold-change  $\geq 1.5$  in the in vitro system were considered. Blue colour depicts data from the NB in vitro system without MYCN induction (A) or from MYCN normal tumors (B). Red colour depicts data from the NB in vitro system with MYCN induction (A) or from tumors with *MYCN* amplification (B).

#### Supplemental figure 2

Box plots demonstrating significantly higher expression of HK2, BZW2 and RPTOR in *MYCN*-amplified (MNA) compared to *MYCN* single copy tumors (*MYCN* sc). Expression levels were deduced from re-analyses of microarray data using an independent set of primary neuroblastoma (GEO database acc. no. GSE32664).

#### Acknowledgements:

Part of this work was supported by Deutsche Forschungsgemeinschaft (DFG) within the Collaborative Research Center SFB 876 "Providing Information by Resource-Constrained Analysis", subprojects B1 "Spectra" to A.S. and C1 "DimRed" to S.R.. The authors want to thank Melanie Baumann and Sabine Dreesmann for excellent technical assistance and Harald Stephan for preparing the figures.

Disclosures: The authors declare that no conflict of interest has to be reported associated with this manuscript.

## References

1. London WB, Castel V, Monclair T, Ambros PF, Pearson AD, Cohn SL, Berthold F, Nakagawara A, Ladenstein RL, Iehara T, Matthay KK. Clinical and biologic features predictive of survival after relapse of neuroblastoma: a report from the International Neuroblastoma Risk Group project. *J Clin Oncol* 2011;29:3286-92.
2. Baker DL, Schmidt ML, Cohn SL, Maris JM, London WB, Buxton A, Stram D, Castleberry RP, Shimada H, Sandler A, Shamberger RC, Look AT, et al. Outcome after reduced chemotherapy for intermediate-risk neuroblastoma. *N Engl J Med* 2010;363:1313-23.
3. Hero B, Simon T, Spitz R, Ernestus K, Gnekow AK, Scheel-Walter HG, Schwabe D, Schilling FH, Benz-Bohm G, Berthold F. Localized infant neuroblastomas often show spontaneous regression: results of the prospective trials NB95-S and NB97. *J Clin Oncol* 2008;26:1504-10.
4. Goto S, Umehara S, Gerbing RB, Stram DO, Brodeur GM, Seeger RC, Lukens JN, Matthay KK, Shimada H. Histopathology (International Neuroblastoma Pathology Classification) and MYCN status in patients with peripheral neuroblastic tumors: a report from the Children's Cancer Group. *Cancer* 2001;92:2699-708.
5. Seeger RC, Brodeur GM, Sather H, Dalton A, Siegel SE, Wong KY, Hammond D. Association of multiple copies of the N-myc oncogene with rapid progression of neuroblastomas. *N Engl J Med* 1985;313:1111-6.
6. Molenaar JJ, Koster J, Zwijnenburg DA, van Sluis P, Valentijn LJ, van der Ploeg I, Hamdi M, van Nes J, Westerman BA, van Arkel J, Ebus ME, Haneveld F, et al. Sequencing of neuroblastoma identifies chromothripsis and defects in neuritogenesis genes. *Nature* 2012.
7. Chen Y, Takita J, Choi YL, Kato M, Ohira M, Sanada M, Wang L, Soda M, Kikuchi A, Igarashi T, Nakagawara A, Hayashi Y, et al. Oncogenic mutations of ALK kinase in neuroblastoma. *Nature* 2008;455:971-4.
8. George RE, Sanda T, Hanna M, Frohling S, Luther W, 2nd, Zhang J, Ahn Y, Zhou W, London WB, McGrady P, Xue L, Zozulya S, et al. Activating mutations in ALK provide a therapeutic target in neuroblastoma. *Nature* 2008;455:975-8.
9. Janoueix-Lerosey I, Lequin D, Brugieres L, Ribeiro A, de Pontual L, Combaret V, Raynal V, Puisieux A, Schleiermacher G, Pierron G, Valteau-Couanet D, Frebourg T, et al. Somatic and germline activating mutations of the ALK kinase receptor in neuroblastoma. *Nature* 2008;455:967-70.
10. Mosse YP, Laudenslager M, Longo L, Cole KA, Wood A, Attiyeh EF, Laquaglia MJ, Sennett R, Lynch JE, Perri P, Laureys G, Speleman F, et al. Identification of ALK as a major familial neuroblastoma predisposition gene. *Nature* 2008;455:930-5.
11. Caren H, Abel F, Kogner P, Martinsson T. High incidence of DNA mutations and gene amplifications of the ALK gene in advanced sporadic neuroblastoma tumours. *The Biochemical journal* 2008;416:153-9.
12. Mosse YP, Laudenslager M, Khazi D, Carlisle AJ, Winter CL, Rappaport E, Maris JM. Germline PHOX2B mutation in hereditary neuroblastoma. *Am J Hum Genet.* 2004;75:727-30.
13. van Limpt V, Schramm A, van Lakeman A, Sluis P, Chan A, van Noesel M, Baas F, Caron H, Eggert A, Versteeg R. The Phox2B homeobox gene is mutated in sporadic neuroblastomas. *Oncogene* 2004;23:9280-8.
14. Buckley PG, Alcock L, Bryan K, Bray I, Schulte JH, Schramm A, Eggert A, Mestdagh P, De Preter K, Vandesompele J, Speleman F, Stallings RL. Chromosomal and microRNA expression patterns reveal biologically distinct subgroups of 11q- neuroblastoma. *Clin Cancer Res* 2010;16:2971-8.
15. Caren H, Kryh H, Nethander M, Sjoberg RM, Trager C, Nilsson S, Abrahamsson J, Kogner P, Martinsson T. High-risk neuroblastoma tumors with 11q-deletion display a poor

prognostic, chromosome instability phenotype with later onset. *Proc Natl Acad Sci U S A* 2010;107:4323-8.

16. Schulte JH, Marschall T, Martin M, Rosenstiel P, Mestdagh P, Schlierf S, Thor T, Vandesompele J, Eggert A, Schreiber S, Rahmann S, Schramm A. Deep sequencing reveals differential expression of microRNAs in favorable versus unfavorable neuroblastoma. *Nucleic Acids Res* 2010;38:5919-28.

17. Schulte JH, Schowe B, Mestdagh P, Kaderali L, Kalaghatgi P, Schlierf S, Vermeulen J, Brockmeyer B, Pajtler K, Thor T, de Preter K, Speleman F, et al. Accurate prediction of neuroblastoma outcome based on miRNA expression profiles. *Int J Cancer* 2010;127:2374-85.

18. Mestdagh P, Bostrom AK, Impens F, Fredlund E, Van Peer G, De Antonellis P, von Stedingk K, Ghesquiere B, Schulte S, Dews M, Thomas-Tikhonenko A, Schulte JH, et al. The miR-17-92 microRNA cluster regulates multiple components of the TGF-beta pathway in neuroblastoma. *Mol Cell* 2010;40:762-73.

19. Schulte JH, Horn S, Otto T, Samans B, Heukamp LC, Eilers UC, Krause M, Astrahantseff K, Klein-Hitpass L, Buettner R, Schramm A, Christiansen H, et al. MYCN regulates oncogenic MicroRNAs in neuroblastoma. *Int J Cancer* 2008;122:699-704.

20. Ross RA, Spengler BA, Biedler JL. Coordinate morphological and biochemical interconversion of human neuroblastoma cells. *J Natl Cancer Inst* 1983;71:741-7.

21. Schweigerer L, Breit S, Wenzel A, Tsunamoto K, Ludwig R, Schwab M. Augmented MYCN expression advances the malignant phenotype of human neuroblastoma cells. Evidence for induction of autocrine growth activity. *Cancer Res.* 1990;50:4411-6.

22. Schulte JH, Schramm A, Klein-Hitpass L, Klenk M, Wessels H, Hauffa BP, Eils J, Eils R, Brodeur GM, Schweigerer L, Havers W, Eggert A. Microarray analysis reveals differential gene expression patterns and regulation of single target genes contributing to the opposing phenotype of TrkA- and TrkB-expressing neuroblastomas. *Oncogene* 2005;24:165-77.

23. Klostermeier UC, Barann M, Wittig M, Hasler R, Franke A, Gavrilova O, Kreck B, Sina C, Schilhabel MB, Schreiber S, Rosenstiel P. A tissue-specific landscape of sense/antisense transcription in the mouse intestine. *BMC genomics* 2011;12:305.

24. Benjamini Y, Hochberg Y. Controlling the False Discovery Rate - a Practical and Powerful Approach to Multiple Testing. *J Roy Stat Soc B Met* 1995;57:289-300.

25. Storey JD. A direct approach to false discovery rates. *J. Roy. Statist. Soc. B.* 2002;64:479-98.

26. Zeller KI, Jegga AG, Aronow BJ, O'Donnell KA, Dang CV. An integrated database of genes responsive to the Myc oncogenic transcription factor: identification of direct genomic targets. *Genome Biol* 2003;4:R69.

27. Murphy DM, Buckley PG, Bryan K, Das S, Alcock L, Foley NH, Prenter S, Bray I, Watters KM, Higgins D, Stallings RL. Global MYCN transcription factor binding analysis in neuroblastoma reveals association with distinct E-box motifs and regions of DNA hypermethylation. *PLoS ONE* 2009;4:e8154.

28. Marschall T, Rahmann S. MoSDi: Motif Statistics and Discovery 2009.

29. Weiss WA, Aldape K, Mohapatra G, Feuerstein BG, Bishop JM. Targeted expression of MYCN causes neuroblastoma in transgenic mice. *EMBO J* 1997;16:2985-95.

30. Gerlinger M, Rowan AJ, Horswell S, Larkin J, Endesfelder D, Gronroos E, Martinez P, Matthews N, Stewart A, Tarpey P, Varela I, Phillimore B, et al. Intratumor heterogeneity and branched evolution revealed by multiregion sequencing. *N Engl J Med* 2012;366:883-92.

31. Parsons DW, Li M, Zhang X, Jones S, Leary RJ, Lin JC, Boca SM, Carter H, Samayoa J, Bettegowda C, Gallia GL, Jallo GI, et al. The genetic landscape of the childhood cancer medulloblastoma. *Science* 2011;331:435-9.

32. Zhang J, Benavente CA, McEvoy J, Flores-Otero J, Ding L, Chen X, Ulyanov A, Wu G, Wilson M, Wang J, Brennan R, Rusch M, et al. A novel retinoblastoma therapy from genomic and epigenetic analyses. *Nature* 2012;481:329-34.
33. Mestdagh P, Fredlund E, Pattyn F, Schulte JH, Muth D, Vermeulen J, Kumps C, Schlierf S, De Preter K, Van Roy N, Noguera R, Laureys G, et al. MYCN/c-MYC-induced microRNAs repress coding gene networks associated with poor outcome in MYCN/c-MYC-activated tumors. *Oncogene* 2010;29:1394-404.
34. Wei JS, Song YK, Durinck S, Chen QR, Cheuk AT, Tsang P, Zhang Q, Thiele CJ, Slack A, Shohet J, Khan J. The MYCN oncogene is a direct target of miR-34a. *Oncogene* 2008.
35. Bernard D, Prasanth KV, Tripathi V, Colasse S, Nakamura T, Xuan Z, Zhang MQ, Sedel F, Jourdain L, Couplier F, Triller A, Spector DL, et al. A long nuclear-retained non-coding RNA regulates synaptogenesis by modulating gene expression. *EMBO J* 2010;29:3082-93.
36. Kogo R, Shimamura T, Mimori K, Kawahara K, Imoto S, Sudo T, Tanaka F, Shibata K, Suzuki A, Komune S, Miyano S, Mori M. Long noncoding RNA HOTAIR regulates polycomb-dependent chromatin modification and is associated with poor prognosis in colorectal cancers. *Cancer Res* 2011;71:6320-6.
37. Niinuma T, Suzuki H, Nojima M, Noshio K, Yamamoto H, Takamaru H, Yamamoto E, Maruyama R, Nobuoka T, Miyazaki Y, Nishida T, Bamba T, et al. Upregulation of miR-196a and HOTAIR Drive Malignant Character in Gastrointestinal Stromal Tumors. *Cancer Res* 2012;72:1126-36.
38. Schramm A, Schulte JH, Klein-Hitpass L, Havers W, Sieverts H, Berwanger B, Christiansen H, Warnat P, Brors B, Eils J, Eils R, Eggert A. Prediction of clinical outcome and biological characterization of neuroblastoma by expression profiling. *Oncogene* 2005;24:7902-12.
39. Guo X, Chen QR, Song YK, Wei JS, Khan J. Exon array analysis reveals neuroblastoma tumors have distinct alternative splicing patterns according to stage and MYCN amplification status. *BMC Med Genomics* 2011;4:35.
40. Qing G, Skuli N, Mayes PA, Pawel B, Martinez D, Maris JM, Simon MC. Combinatorial regulation of neuroblastoma tumor progression by N-Myc and hypoxia inducible factor HIF-1alpha. *Cancer Res* 2010;70:10351-61.
41. Boon K, Caron HN, van Asperen R, Valentijn L, Hermus MC, van Sluis P, Roobeek I, Weis I, Voute PA, Schwab M, Versteeg R. N-myc enhances the expression of a large set of genes functioning in ribosome biogenesis and protein synthesis. *EMBO J* 2001;20:1383-93.
42. Krasnoselsky AL, Whiteford CC, Wei JS, Bilke S, Westermann F, Chen QR, Khan J. Altered expression of cell cycle genes distinguishes aggressive neuroblastoma. *Oncogene* 2005;24:1533-41.
43. Johnsen JI, Segerstrom L, Orrego A, Elfman L, Henriksson M, Kagedal B, Eksborg S, Sveinbjornsson B, Kogner P. Inhibitors of mammalian target of rapamycin downregulate MYCN protein expression and inhibit neuroblastoma growth in vitro and in vivo. *Oncogene* 2008;27:2910-22.
44. Segerstrom L, Baryawno N, Sveinbjornsson B, Wickstrom M, Elfman L, Kogner P, Johnsen JI. Effects of small molecule inhibitors of PI3K/Akt/mTOR signaling on neuroblastoma growth in vitro and in vivo. *Int J Cancer* 2011;129:2958-65.

Table 1

Database/Motif	Upregulated MYCN targets	Downregulated MYCN targets
MYCNot	HK2	ITM2C CD44
MycDB	U5-RNA SCML2 HK2	MEIS1 LAMP2 GABARAP SERPINB1 TMSB4X
E-Box overrepresented in promoter	SNORA76 (CACGTG) SNORD6 (CATGTG) SNORD77 (CATTTG) PTCH2 (CATTTG) SCML2 (CATCTG)	CD44 (CATGTG)

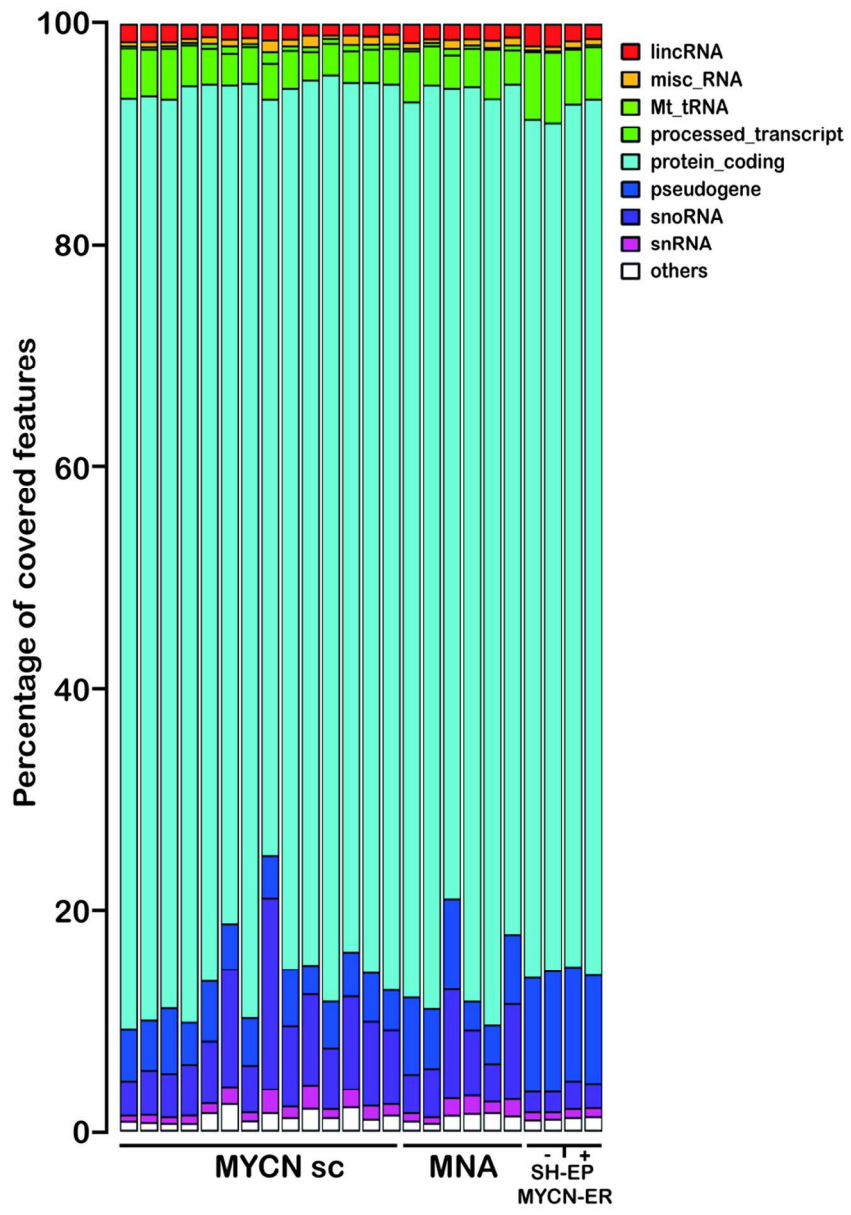


Figure 1  
89x123mm (300 x 300 DPI)

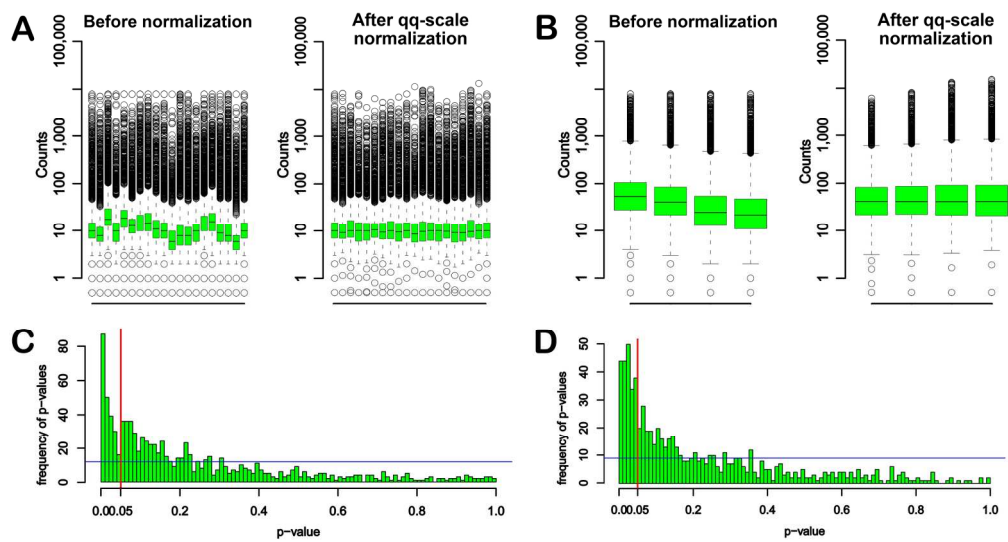


Figure 2  
93x49mm (600 x 600 DPI)

## Unable to Convert Image

The dimensions of this image (in pixels) are too large to be converted. For this image to convert, the total number of pixels (height x width) must be less than 40,000,000 (40 megapixels).

Figure 3

## Unable to Convert Image

The dimensions of this image (in pixels) are too large to be converted. For this image to convert, the total number of pixels (height x width) must be less than 40,000,000 (40 megapixels).

Figure 4

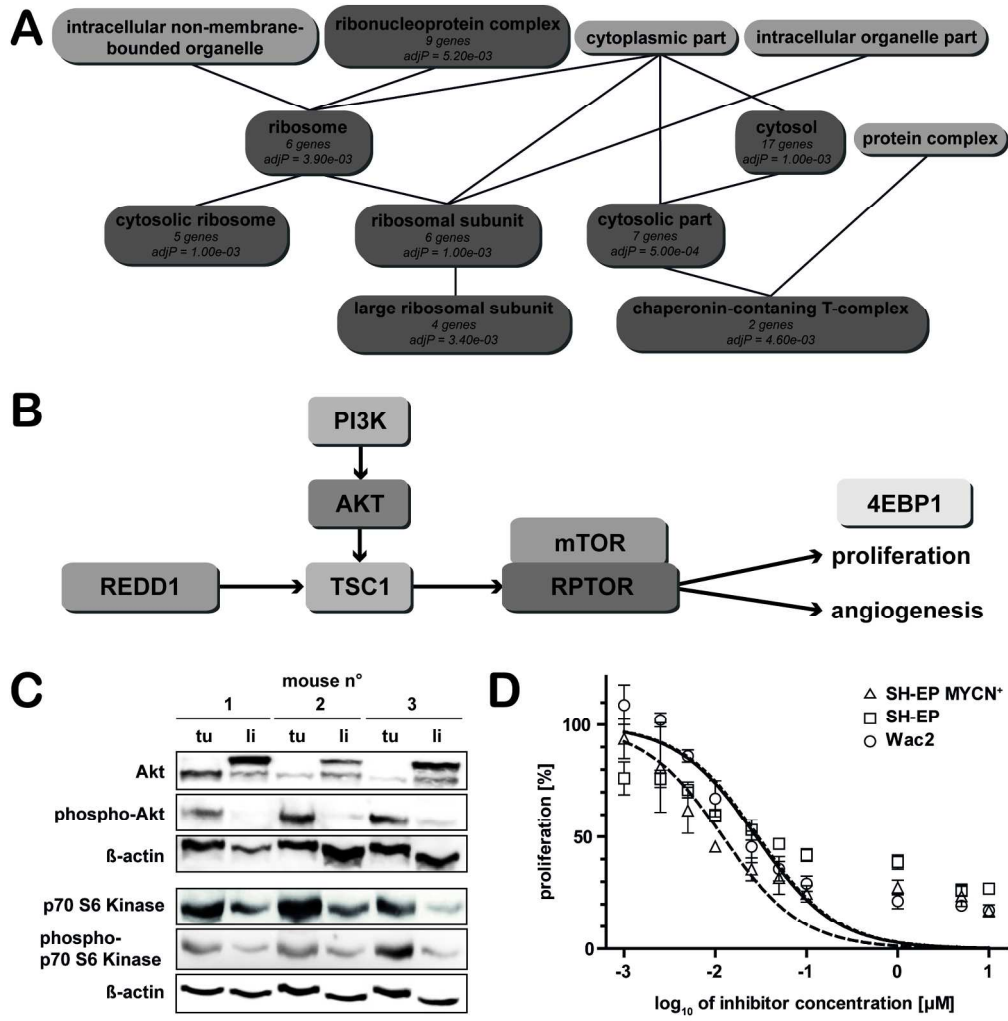


Figure 5  
178x181mm (300 x 300 DPI)